Received: 17 June 2022 | Revised: 26 July 2022 | Accepted: 5 August 2022

DOI: 10.1111/jace.18720

Journal of the American Ceramic Society

RESEARCH ARTICLE

Effect of material parameters on thermal shock crack of ceramics calculated by phase-field method

Chuandong Zuo[1,3] | **Qingxian Li**[1,3] | **Qian Wang**[2] | **Yuqiao Li**[1,3] | **Long Li**[1,3] | **Jiachen Wei**[1,3] | **Yingfeng Shao**[1,3] | **Fan Song**[1,3]

[1]State Key Laboratory of Nonlinear Mechanics and Beijing Key Laboratory of Engineered Construction and Mechanobiology, Institute of Mechanics, Chinese Academy of Sciences, Beijing, China

[2]Ganjiang Innovation Academy, Chinese Academy of Sciences, Ganzhou, China

[3]School of Engineering Science, University of Chinese Academy of Sciences, Beijing, China

Correspondence
Yingfeng Shao and Fan Song, State Key Laboratory of Nonlinear Mechanics and Beijing Key Laboratory of Engineered Construction and Mechanobiology, Institute of Mechanics, Chinese Academy of Sciences, Beijing 100190, China.
Email: shaoyf@lnm.imech.ac.cn and songf@lnm.imech.ac.cn

Funding information
National Natural Science Foundations of China, Grant/Award Numbers: 11972041, 51504165); Youth Innovation Promotion Association of the Chinese Academy of Sciences

Abstract

Based on alumina ceramics, we employ the phase-field method to study the effects of thermal conductivity, specific heat, density, thermal expansion coefficient, Young's modulus, and fracture toughness on thermal shock cracks. The results show that increasing thermal conductivity and fracture toughness will reduce thermal shock damage. That is, the long crack length becomes shorter, or the crack density becomes smaller. However, increasing the thermal expansion coefficient and Young's modulus will increase thermal shock damage. It is consistent with the previous thermal shock theory. The effect of material parameters on crack propagation speed was also considered. In addition, we carried out a thermal shock test of the zirconia. The results of the phase-field calculation are the same as the thermal shock results of the zirconia. This paper verifies that the phase-field method is suitable for simulating thermal shock cracks in other ceramics.

KEYWORDS

ceramic, crack pattern, material parameters, phase-field, thermal shock

1 | INTRODUCTION

Ceramics are extensively used in the aerospace industry instead of metals because of their excellent high-temperature properties.[1–4] However, due to the brittleness of ceramics, it is easy to fail due to thermal shock when the ambient temperature changes sharply, which is the inherent disadvantage of ceramic materials.[3,4]

Due to the complexity of the multi-field coupling fracture in thermal shock, the simulation analysis of fracture-induced failure plays an important role in designing materials or structures. In recent 10 years, there have been some theoretical models to study thermal shock crack initiation and propagation of ceramics, including phase-field,[5–10] meso-damage,[11,12] energy minimization,[13] nonlocal failure,[14] bond-based peridynamic,[15] and gradient damage.[16,17] These theoretical works verify and complement each other and have achieved remarkable scientific progress.

Because the phase-field method does not need additional discontinuity and tracking of the crack surface, it is very convenient to calculate ceramic thermal shock. For example, Mandala,[5] Tangella,[6] Chu,[7] and Wang[8] calculated the thermal shock crack of alumina by the phase-field

method and obtained the same conclusion as the test, however, due to the limitations of the thermal shock test. The previous phase-field method mainly focuses on the thermal shock test of alumina ceramics, and there are almost no other ceramics. Besides, few studies have been conducted to study the effects of different materials or different material parameters on thermal shock crack growth. It hinders the applications of the phase-field method to other materials. Therefore, it is urgent to understand the effect of material parameters on thermal shock crack propagation and verify that the phase-field method can predict the thermal shock damage of other ceramics.

The present paper studied the effects of thermal conductivity, specific heat, density, thermal expansion coefficient, Young's modulus, and fracture toughness of materials on thermal shock cracks by phase-field method and compared with the previous thermal shock theory.[18,19] In addition, by verifying the thermal shock crack of zirconia, we believe that the phase-field method should be suitable for simulating thermal shock cracks of other ceramics.

2 | EXPERIMENT

2.1 | Materials and preparation

Alumina ceramic (grain size 7.5 μm; Jiawei Ceramics Co., Ltd., Zhuhai, China) was prepared by tape casting and sintered at 1650°C for 2 h without pressure. 3Y–ZrO_2 ceramic (grain size 0.6 μm; Jiawei Ceramics Co., Ltd., Zhuhai, China) was also prepared by tape casting and sintered at 1450°C for 2 h without pressure. The microstructure of the ceramics was characterized using scanning electron microscopy (SEM, Tescan Amber, Brünn, Czech Republic). The relative density of Al_2O_3 and 3Y–ZrO_2 was about 98% and 99%, respectively, by calculation from measured weight and dimension.

2.2 | Thermal shock process

We employed the ceramic sheets with 1.0 mm × 10 mm × 50 mm to study the thermal shock crack morphology by water quenching. We stacked the sample with four identical ceramic slabs and bound them up with Inconel wires from both ends of the slabs to prevent water access to the side faces, as shown in Figure 1. We heated the sample to the test temperature and held that temperature for 30 min. Then, we dropped the specimen into a 20°C water bath. Taken out and dried, we impregnated the specimens with blue ink to observe the cracks morphology after quenching. We studied the crack patterns in the face of 10 mm × 50 mm using digital scanning.

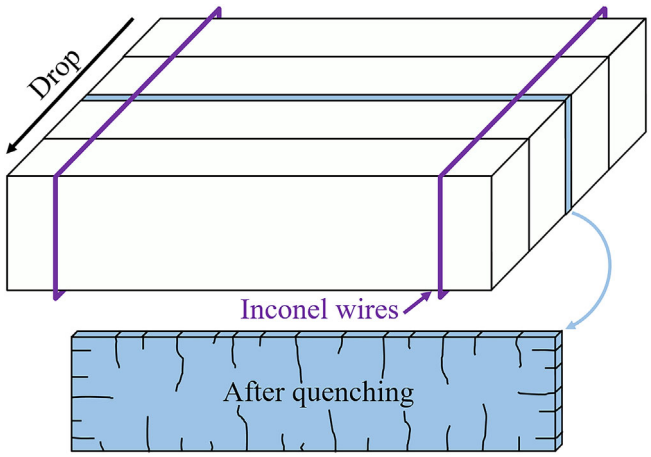

FIGURE 1 Bound specimen for thermal shock test

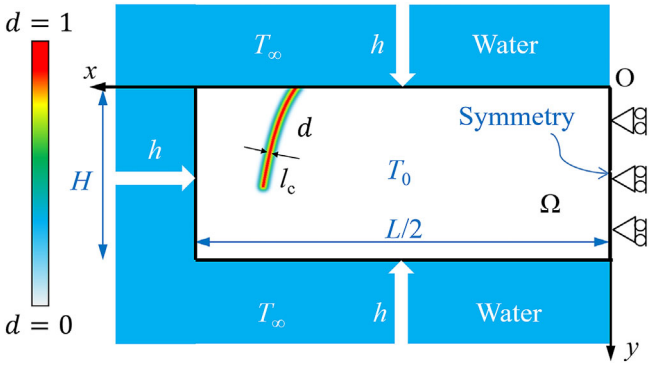

FIGURE 2 The phase-field model simulates the ceramic crack under thermal shock. d is the phase-field by which the internal discrete crack is approximated as a diffusive crack topology, and l_c is the width of the diffusive crack.

2.3 | Phase-field model for thermal shock

The present study uses a thermal–mechanical coupled phase-field model to simulate the thermal shock crack under thermal shock loading.[20] The experimental condition allows us to regard the thermal–mechanical field as two-dimensional, and surfaces of the model are subjected to convective heat transfer, as illustrated in Figure 2. In the phase-field model, the crack is considered a discrete crack by a scalar phase-field variable d with $d = 0$ means the ceramic is intact, and $d = 1$ means the ceramic is wholly damaged. l_c represents the width of the crack, as illustrated in Figure 2.

According to Shao et al.,[21] quenching crack propagation can be considered a quasistatic process. Then the free energy density of thermoelastic solid for our problem

TABLE 1 Mechanical and thermal parameters of alumina and zirconia used in calculation

Ceramic	Young modulus E (GPa)	Poisson's ratio ν	Fracture toughness K_{IC} (MPa m$^{1/2}$)	Coefficient of thermal expansion α (10^{-6} K^{-1})	Ref.
Al_2O_3	370	0.22	3.8	Figure 3C	25
3Y–ZrO_2	200	0.3	5	11.7	23

contains elastic strain energy, fracture energy, and thermal energy can be defined as[20,22]

$$\psi(\mathbf{u}, T, d) = \int_\Omega \left(g(d)\psi_0^+(\boldsymbol{\varepsilon}^e) + \psi_0^-(\boldsymbol{\varepsilon}^e)\right)dV + \int_\Omega \frac{G_c}{2l_c}\left(d^2 + l_c^2|\nabla d|^2\right)dV - \int_\Omega \left(\rho c T \ln\frac{T}{T_0}\right)dV \quad (1)$$

where $\mathbf{u}$, T, T_0, G_c, c, and ρ are displacement, temperature, critical energy release rate, reference temperature, specific heat, and density, respectively; $\boldsymbol{\varepsilon}^e = \boldsymbol{\varepsilon} - \boldsymbol{\varepsilon}^T$ is the elastic strain tensor, where $\boldsymbol{\varepsilon}$ and $\boldsymbol{\varepsilon}^T$ are total strain and thermal strain; $g(d) = (1-d)^2 + \delta$ is the degradation function, and δ is a parameter chosen to be as small as possible to ensure the problem converges; $\psi_0^+(\boldsymbol{\varepsilon}^e)$ and $\psi_0^-(\boldsymbol{\varepsilon}^e)$ are the tensile and compressive parts of the elastic energy density[23]:

$$\psi_0^\pm(\boldsymbol{\varepsilon}^e) = \frac{\lambda}{2}\langle tr\boldsymbol{\varepsilon}^e\rangle_\pm^2 + \mu\sum_{i=1}^3 \left\langle \varepsilon_i^e\right\rangle_\pm^2 \quad (2)$$

with $<a>_\pm = 1/2(a \pm |a|)$, λ and μ are the Lamé constants, $\varepsilon_i^e (i = 1, 2, 3)$ values are the principal elastic strains. Minimizing the system's free energy, we can get the governing equation for the phase-field evolution:

$$\frac{G_c}{l_c}\left(d - l_c^2\nabla^2 d\right) = 2(1-d)\mathcal{H} \quad (3)$$

where $\mathcal{H} = \max_{s\in[0,t]}(\psi_+)$ is a local history field of the maximum energy density to ensure that the crack growth is irreversible.

Then, combining the momentum conservation equation and heat transfer equation, we can obtain the governing equations of our problem's evolution of the displacement, phase, and temperature fields. Discretized the governing equations by finite element, we can obtain numerical solutions to our problem. Details are described elsewhere, and this method has given a good description of the thermal shock crack of Al_2O_3.[6–8]

The model's dimensions are $L = 50$ mm and $H = 10$ mm in the X and Y directions, respectively. The left 1/2 area of this model is shown in Figure 2. The size of the finite element is 0.012 mm, and the input parameters of ceramics used in the simulation are listed in Table 1. To make simulation consistent with the actual situation, the thermal conductivity and specific heat of two ceramics and the thermal expansion coefficient of Al_2O_3 were considered temperature-dependent in the range 20–500°C,[24–26] as shown in Figure 3. The length-scale parameter is chosen as $l_c = 0.05$ mm. The convective heat transfer coefficient h of ceramics at the critical thermal shock temperature, 400 and 500°C are 40 000, 86 000, and 57 000 W/m^2 K used in the calculation,[13,27] respectively.

In the phase-field method, there is a relationship among G_c, σ_T (tensile strength), and l_c. As the parameter l_c is also a numerical parameter to adjust the damage concentration, the choice of l_c is not entirely arbitrary. Therefore, if this relationship is maintained, G_c and σ_T are usually slightly different from the actual material constant. Because the critical thermal shock temperature difference, ΔT_c, is also important, we use appropriate G_c and l_c values to relatively accurately predict the ΔT_c and crack propagation under other temperature differences. It makes the simulation calculation more reasonable.

3 | RESULTS AND DISCUSSIONS

3.1 | Comparison and verification of thermal shock test

The comparison between numerical and experimental results of cracks in ceramics after thermal shock is shown in Figure 4. We can see that they have a similar crack classification structure. The comparison of crack density and long crack length between the experiment and calculation is shown in Figure 5. We can see that the numerical test results have the consistency of crack array length and density with the experimental results. In addition, the comparison result of alumina is very similar to the previous comparison results.[6–8] Note that, it is difficult to distinguish the crack with a length less than 0.2 mm, so we removed these cracks in the statistical simulation and test crack data. We calculated the crack density by dividing the total number of cracks on the upper and lower sides by the total length of both sides and selected the longest nine longitudinal cracks for comparison because of the crack morphology.

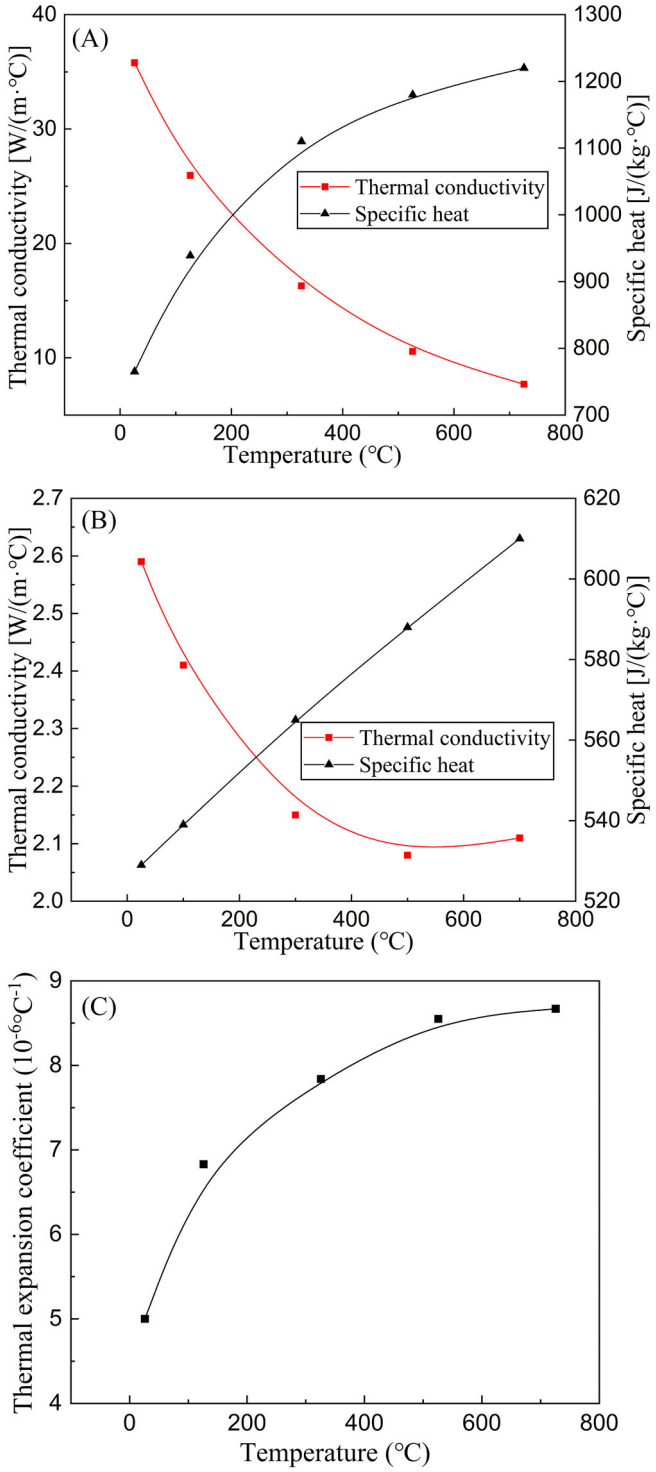

FIGURE 3 Thermal conductivity and specific heat of (A) Al_2O_3,[22] (B) 3Y–ZrO_2,[23] and thermal expansion coefficient of (C) Al_2O_3[24] versus temperature used in the calculation

We used the phase-field method to calculate the ΔT_c of Al_2O_3 and 3Y–ZrO_2. The calculation results are shown in Figure S1. The ΔT_c value of Al_2O_3 is about 170°C, whereas that of 3Y–ZrO_2 is about 235°C. It is very close to our experimental results that the ΔT_c value of Al_2O_3 is about 180°C, and that of 3Y–ZrO_2 is about 260°C. The previous results show that the phase-field method is suitable for thermal shock simulation of ceramics.

The classical theory of thermoelasticity considers that thermal conductivity, specific heat, coefficient of thermal expansion, and Young's modulus affect the thermal stress during the process of thermal shock.[28] Therefore, we consider the effect of the previous material parameters, including fracture toughness, in the thermal shock crack calculation by the phase-field method. Based on alumina, we change one parameter's values by 0.5, 1, or 2 times for each calculation, and the other parameters remain unchanged. The calculated thermal shock temperature difference ΔT is 380°C.

3.2 | Effect of thermal conductivity

The thermal shock crack pattern variation with thermal conductivity k calculated by the phase-field method is shown in Figure 6. We can see that the number of cracks decreases obviously with the increase of k. The variation of crack density and long crack length with k is shown in Figure 7. As indicated, increasing k reduces the crack density after crack propagation, whereas the crack length decreases slightly. From the perspective of fracture mechanics, it will increase the residual mechanical properties of the sample. That is, the damage to the material is reduced. It is close to the traditional rule that materials with higher k will have better thermal shock resistance.[29] However, our water quenching is a relatively violent thermal shock process. The Biot module $\beta = rh/k \approx 27 \gg 1$, where $r = 5$ mm is a characteristic body dimension in the direction of the maximum temperature gradient. So, according to Wang's research,[29] the effect of the increase in thermal conductivity becomes smaller.

3.3 | Effect of specific heat or density

The thermal shock crack pattern variation with specific heat c and density ρ calculated by the phase-field method is shown in Figure 8. The result shows that the thermal shock crack pattern obtained by changing c or ρ is the same. According to classical heat transfer theory, the temperature field of plate heat transfer is only related to β and thermal diffusivity $a = k/\rho c$.[30] Because the change of a caused by the change of c or ρ is the same, their crack morphology is the same. In addition, it is difficult to see the law of the crack pattern changing with parameters is at first glance. The variation of crack density and long crack length with c or ρ is shown in Figure 7. We can see that

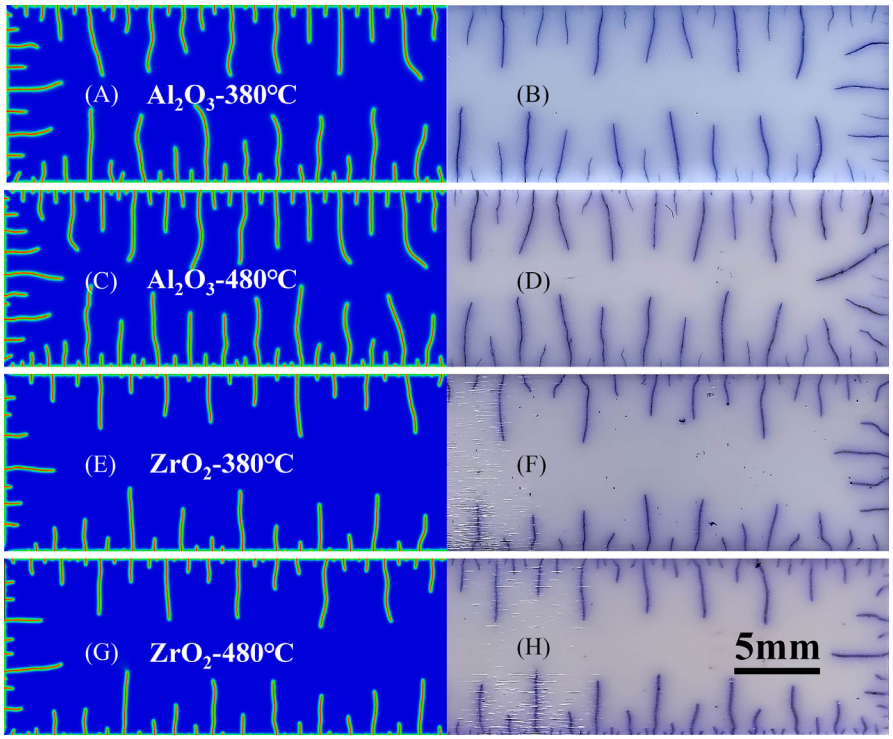

FIGURE 4 The comparison between the crack pattern of ceramics after the thermal shock with temperature difference ΔT and the calculation of the phase-field method: (A) Al_2O_3 simulation result of $\Delta T = 380°C$; (B) Al_2O_3 experimental result of $\Delta T = 380°C$; (C) Al_2O_3 simulation result of $\Delta T = 480°C$; (D) Al_2O_3 experimental result of $\Delta T = 480°C$; (E) 3Y–ZrO_2 simulation result of $\Delta T = 380°C$; (F) 3Y–ZrO_2 experimental result of $\Delta T = 380°C$; (G) 3Y–ZrO_2 simulation result of $\Delta T = 480°C$; and (H) 3Y–ZrO_2 experimental result of $\Delta T = 480°C$

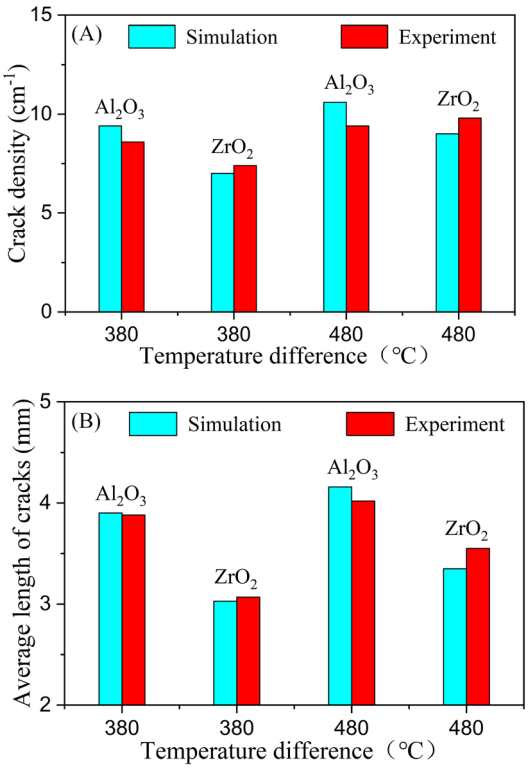

FIGURE 5 (A) Crack density and (B) long crack length of two ceramics after thermal shock with different temperature differences, and the comparison with phase-field calculation

long crack length and crack density are unchanged with the increase of specific heat or density; that is, the thermal shock damage is not sensitive to the changes of the previous two parameters.

3.4 | Effect of thermal expansion coefficient, Young's modulus, or fracture toughness

The variation of thermal shock crack pattern with thermal expansion coefficient α, Young's modulus E, and fracture toughness K_{IC} calculated by the phase-field method is shown in Figure 9. We can see that the thermal shock crack pattern obtained by changing α or E is the same. The changing trend of the thermal shock crack pattern obtained by changing K_{IC} is just opposite to the previous one. It is because changing α or E to x times and changing K_{IC} to $1/x$ times will get the same phase-field evolution Equation (3). For example, when K_{IC} becomes $1/x$ times, the energy release rate G_c becomes $1/x^2$ times the original value from $G_C = K_{IC}^2/E$, and the strain energy $\mathcal{H}$ remains unchanged. That is, G_c: $\mathcal{H} = 1$: x^2. When α or E becomes x times the original value, G_c: $\mathcal{H} = 1$: x^2 can also be obtained. Therefore, their crack morphology is the same.

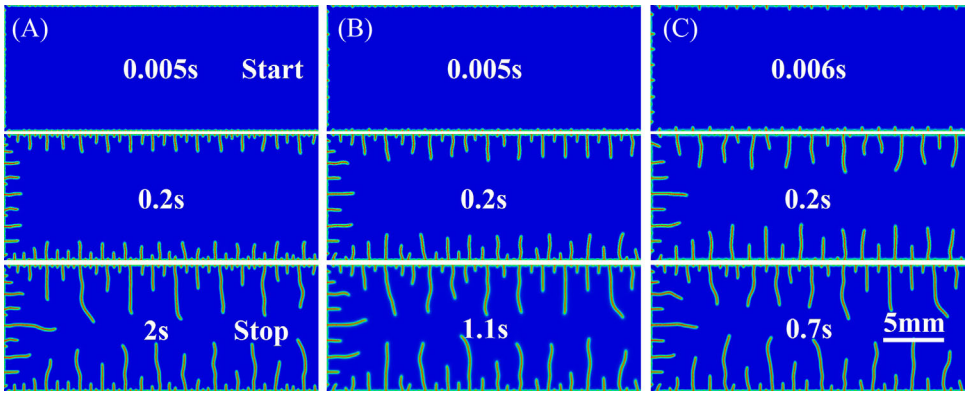

FIGURE 6 Variation of thermal shock crack pattern with thermal conductivity k calculated by phase-field method (A) 0.5k, (B) k, and (C) 2k with the temperature difference of 380°C

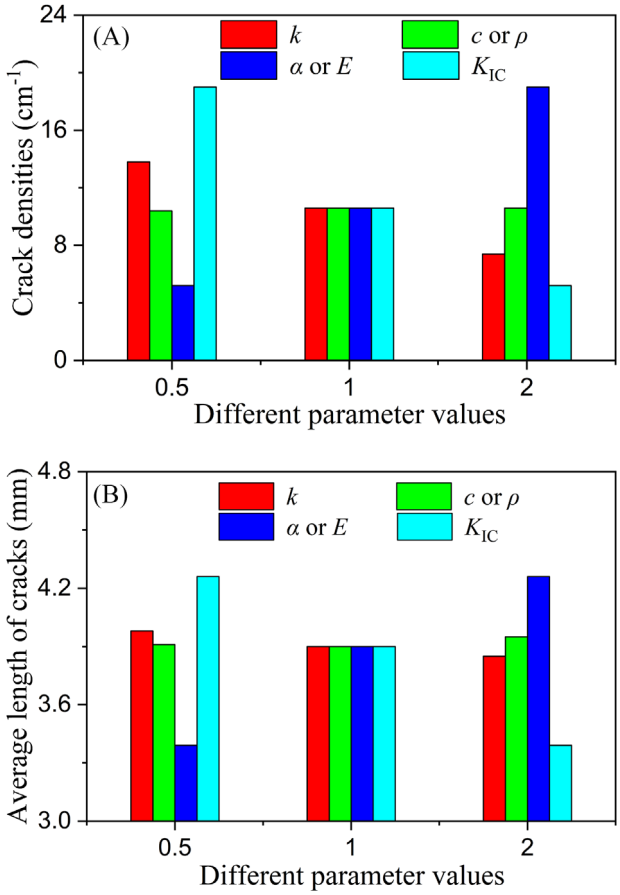

FIGURE 7 The (A) crack density and (B) long crack length calculated by the phase-field method vary with material parameters after the thermal shock of $\Delta T = 380°C$

The change of crack density and long crack length with α, E, and K_{IC} by phase-field calculation is shown in Figure 7. As indicated, with the increase of K_{IC}, the crack density becomes smaller, and the length of the long crack becomes shorter. That is, the damage to the material is reduced. It is consistent with Hasselman's thermal shock damage theory[18]:

$$R^{\upsilon} = \frac{\left(K_{IC}/\sigma_f\right)^2}{1-\upsilon} = \frac{EG_C}{\sigma_f^2(1-\upsilon)} \tag{4}$$

where σ_f is the fracture strength, and υ is the Poisson ratio. When K_{IC} increases, the energy consumed by producing the same crack length increases, so the crack is not easy to expand intuitively.

Because the trend is opposite to that of K_{IC}, with the increase of α or E, the damage of the ceramic increases. It is consistent with the previous research of Hasselman's thermal shock resistance theory[19]:

$$R = \Delta T_c = \frac{\sigma_f(1-\upsilon)}{E\alpha} \tag{5}$$

From Equation (5), with the increase of E, the thermal shock resistance parameter R will decrease, indicating the more prone to thermal shock failure. However, it is inconsistent with Hasselman's thermal shock damage theory (Equation 4). The possible reason is that the influence of E in thermal shock damage theory is more suitable for porous ceramics than dense ceramics.[31]

In addition, we study the influence of material parameters on the crack propagation speed, as shown in Figures 6–9, Video S1–S3, and Table 2. We also selected the longest nine cracks for comparison. We can see that the changes in density or specific heat significantly affect the thermal shock crack propagation speed. The influence of thermal conductivity is slightly smaller. The thermal expansion coefficient, Young's modulus, and fracture toughness least affect the crack propagation speed. We can see that the crack speed is slow, about 10 mm/s, which can be regarded as a quasi-static process.[21] At the

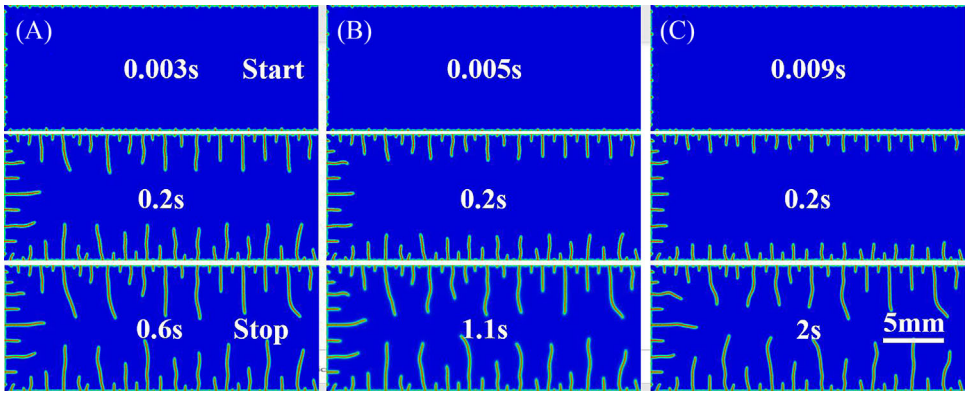

FIGURE 8 Variation of thermal shock crack pattern with specific heat c or density ρ calculated by phase field method (A) $0.5c$ or 0.5ρ, (B) c or ρ, and (C) $2c$ or 2ρ with the temperature difference of 380°C

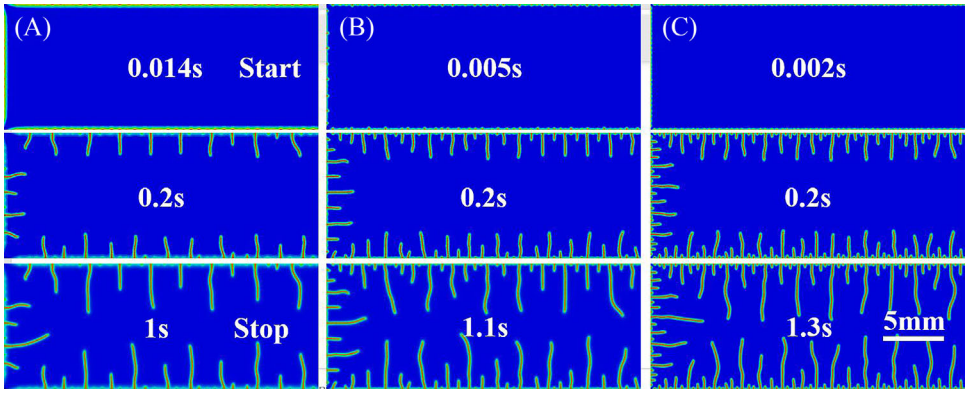

FIGURE 9 Variation of thermal shock crack pattern with thermal expansion coefficient α, Young's modulus E, and fracture toughness K_{IC}, calculated by the phase-field method: (A) 0.5α, $0.5E$, or $2K_{IC}$; (B) α, E, or K_{IC}; and (C) 2α, $2E$, or $0.5K_{IC}$ with the temperature difference of 380°C

TABLE 2 Crack propagation speed of thermal shock with different material parameters under the temperature difference of 380°C

Average speed (mm/s)	Initial	0.5k	2k	0.5c/0.5ρ	2c/2ρ	0.5α/0.5E/2K_{IC}	2α/2E/0.5K_{IC}
0.2 s	9.63 ± 0.49	6.55 ± 0.35	13.6 ± 0.74	14.13 ± 0.32	6.34 ± 0.26	9.11 ± 0.67	10.27 ± 0.42
Whole process	3.56 ± 0.19	2.0 ± 0.14	5.55 ± 0.52	6.55 ± 0.26	1.98 ± 0.17	3.44 ± 0.24	3.28 ± 0.14

same time, we find that the crack propagation speed of Al_2O_3 is faster than that of 3Y–ZrO_2, and the average speed of 0.2 s is a little more than three times that of 3Y–ZrO_2 under the temperature difference of 380°C. Figure 10 shows the SEM of the thermal shock fracture surfaces of the Al_2O_3 and 3Y–ZrO_2, respectively. We can see a mixed mode of intergranular and transgranular fracture from the fracture surfaces, but the intergranular fracture is the primary mode. It is consistent with what was reported by Kobayashi that the slower the crack propagation speed of ceramics, the less the proportion of transgranular fracture.[32]

In a word, the thermal expansion coefficient, Young's modulus, and fracture toughness have the most significant influence on thermal shock damage among the previous parameters; the second is thermal conductivity; the changes in density and specific heat have a minor effect on thermal shock damage. Under the same thermal shock conditions, compared with alumina, zirconia has a shorter crack length and smaller density (Figure 5). It is mainly due to zirconia having higher fracture toughness and lower Young's modulus than alumina, which is consistent with our phase-field calculation. The influence of material parameters on thermal shock crack is verified.

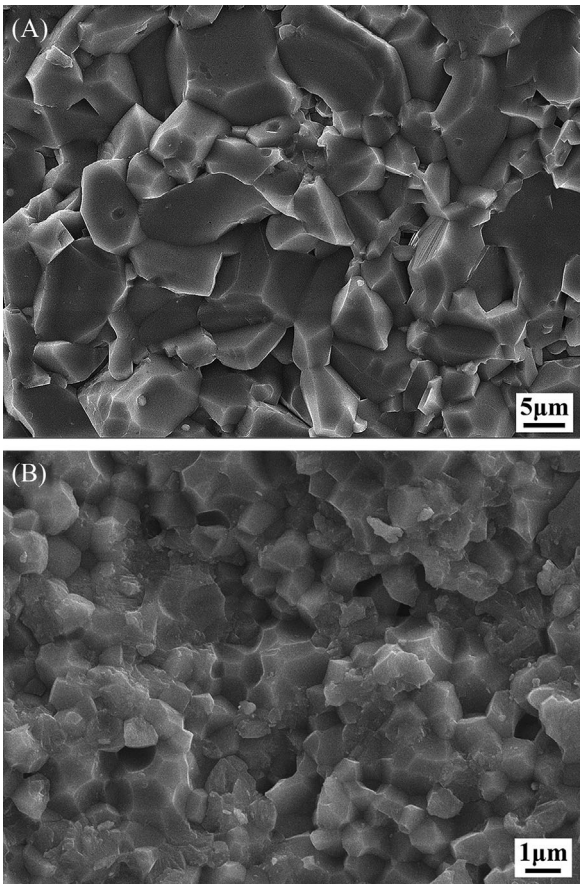

FIGURE 10 Scanning electron microscopy (SEM) of the thermal shock fracture surfaces of (A) Al_2O_3 and (B) 3Y–ZrO_2, respectively

4 | CONCLUSIONS

Based on the successful prediction of the thermal shock results with alumina using the phase-field method, the effects of multiple material parameters on ceramic's thermal shock crack pattern were studied by a phase-field method. The calculation results show that the increase of fracture toughness and thermal conductivity will reduce thermal shock damage; the long crack length becomes shorter, and the crack density becomes smaller. The increase in thermal expansion coefficient and Young's modulus will increase thermal shock damage. Besides, specific heat and density seem not to affect thermal shock damage but have the greatest effect on the crack propagation speed. Among them, the coefficient of thermal expansion, Young's modulus, and fracture toughness have the most significant effect on the thermal shock damage. By comparing the zirconia test, we verify the effectiveness of the phase-field simulation method in calculating thermal shock crack propagation. Therefore, this method should suit thermal shock cracks simulation in many ceramics.

ACKNOWLEDGMENTS

This work was sponsored by the National Natural Science Foundations of China (Grant nos. 11972041 and 51504165) and Youth Innovation Promotion Association CAS.

REFERENCES

1. Danzer R, Lube T, Supancic P, Damani R. Fracture of ceramics. Adv Eng Mater. 2008;10:275–98. https://doi.org/10.1002/adem.200700347
2. Niu ZB, Wang BZ, Pan LJ, Li DX, Jia DC, Yang ZH, et al. Mechanical and thermal shock properties of Cf/SiBCN composite: effect of sintering densification and fiber coating. J Am Ceram Soc. 2022;105:4321–35. https://doi.org/10.1111/jace.18364
3. Zhang PP, Sun YH, Wang YL, Zheng YF, Zhang XF, Zhang QL, et al. Thermal shock resistance of thermal barrier coatings modified by selective laser remelting and alloying techniques. J Am Ceram Soc. 2022;105:6345–58. https://doi.org/10.1111/jace.18586
4. Pompe WE. Thermal shock behavior of ceramic materials-modeling and measurement. In: Schneider GA, Petzow G, editors. Thermal shock and thermal fatigue behavior of advanced ceramics. Springer Netherlands; 1993.
5. Mandala TK, Nguyena VP, Wub JY, Nguyen-Thanhc C, Vaucorbeild A. Fracture of thermo-elastic solids: phase-field modeling and new results with an efficient monolithic solver. Comput Meth Appl Mech Eng. 2021;376:113648. https://doi.org/10.1016/j.cma.2020.113648
6. Tangella RG, Kumbhar P, Annabattula RK. Hybrid phase-field modeling of thermo-elastic crack propagation. Int J Comput Meth Eng Sci Mech. 2021;23:29–44. https://doi.org/10.1080/15502287.2021.1904462
7. Chu DY, Li X, Liu ZL. Study the dynamic crack path in brittle material under thermal shock loading by phase field modeling. Int J Fract. 2017;208:115–30. https://doi.org/10.1007/s10704-017-0220-4
8. Wang T, Ye X, Liu ZL, Liu XM, Chu DY, Zhuang Z. A phase-field model of thermo-elastic coupled brittle fracture with explicit time integration. Comput Mech. 2020;65:1305–21. https://doi.org/10.1007/s00466-020-01820-6
9. Li DY, Li PD, Li WD, Li WG, Zhou K. Three-dimensional phase-field modeling of temperature-dependent thermal shock-induced fracture in ceramic materials. Eng Fract Mech. 2022;268:108444. https://doi.org/10.1016/j.engfracmech.2022.108444
10. McClenny LD, Butt MI, Abdoelatef MG, Pate MJ, Yee KL, Harikrishnan R, et al. Experimentally validated multiphysics modeling of fracture induced by thermal shocks in sintered UO_2 pellets. J Nucl Mater. 2022;565:153719. https://doi.org/10.1016/j.jnucmat.2022.153719
11. Tang SB, Zhang H, Tang CA, Liu HY. Numerical model for the cracking behavior of heterogeneous brittle solids subjected to thermal shock. Int J Solid Struct. 2016;80:520–31. https://doi.org/10.1016/j.ijsolstr.2015.10.012
12. Shao YF, Liu BY, Wang XH, Li L, Wei JC, Song F. Crack propagation speed in ceramic during quenching. J Eur Ceram Soc. 2018;38:2879–85. https://doi.org/10.1016/j.jeurceramsoc.2018.02.028
13. Jiang CP, Wu XF, Li J, Song F, Shao YF, Xu XH, et al. A study of the mechanism of formation and numerical simulations of crack

patterns in ceramics subjected to thermal shock. Acta Mater. 2012;60:4540–50. https://doi.org/10.1016/j.actamat.2012.05.020

14. Li J, Song F, Jiang CP. Direct numerical simulations on crack formation in ceramic materials under thermal shock by using a non-local fracture model. J Eur Ceram Soc. 2013;33:2677–87. https://doi.org/10.1016/j.jeurceramsoc.2013.04.012
15. Wang YT, Zhou XP, Kou MM. An improved coupled thermo-mechanic bondbased peridynamic model for cracking behaviors in brittle solids subjected to thermal shocks. Eur J Mech Solid. 2019;73:282–305. https://doi.org/10.1016/j.euromechsol.2018.09.007
16. Bourdin B, Marigo JJ, Maurini C, Sicsic P. Morphogenesis and propagation of complex cracks induced by thermal shocks. Phys Rev Lett. 2014;112:014301. https://doi.org/10.1103/PhysRevLett.112.014301
17. Sicsic P, Marigo JJ, Maurini C. Initiation of a periodic array of cracks in the thermal shock problem: a gradient damage modeling. J Mech Phys Solid. 2014;63:256–84. https://doi.org/10.1016/j.jmps.2013.09.003
18. Hasselman DP. Elastic energy at fracture and surface energy as design criteria for thermal shock. J Am Ceram Soc. 1963;46:535–40. https://doi.org/10.1111/j.1151-2916.1963.tb14605.x
19. Hasselman DP. Thermal stress resistance parameters for brittle refractory ceramics: a compendium. Am Ceram Soc Bull. 1970;49:1033–7.
20. Miehe C, Schanzel LM, Ulmer H. Phase field modeling of fracture in multi-physics problems. Part I. Balance of crack surface and failure criteria for brittle crack propagation in thermo-elastic solids. Comput Meth Appl Mech Eng. 2015;294:449–85. https://doi.org/10.1016/j.cma.2014.11.016
21. Shao YF, Song F, Liu BY, Li W, Li L, Jiang CP. Observation of ceramic cracking during quenching. J Am Ceram Soc. 2017;100:520–3. https://doi.org/10.1111/jace.14674
22. Han HY, Wang T, Huang GY, Liu ZL, Zhuang Z. Study of spontaneous adiabatic shear bands in expanding rings under explosion by thermo-elastic-plastic phase field model. Int J Impact Eng. 2022;161:104084. https://doi.org/10.1016/j.ijimpeng.2021.104084
23. Miehe C, Welschinger F, Hofacker M. Thermodynamically consistent phase-field models of fracture: variational principles and multi-field FE implementations. Int J Numer Methods Eng. 2010;83:1273–311. https://doi.org/10.1002/nme.2861
24. Bergman TL, Lavine AS, Incropera FP, Dewitt DP. Fundamentals of heat and mass transfer. Hoboken: Wiley; 2011. p. 987.
25. Kondoh J, Shiota H, Kawachi K, Nakatani T. Yttria concentration dependence of tensile strength in yttria-stabilized zirconia. J Alloys Compd. 2004;365:253–8. https://doi.org/10.1016/S0925-8388(03)00640-6
26. Jiang DL, Li LT, Ouyang SX, Shi JL. China materials engineering canon. In: Shi CX, Zhong QP, Li CG,editors. Beijing: Chemical Industry Press;. 2006. p. 35.
27. Shao YF, Du RQ, Wu XF, Song F, Xu XH, Jiang CP. Effect of porosity on the crack pattern and residual strength of ceramics after quenching. J Mater Sci. 2013;48:6431–36. https://doi.org/10.1007/s10853-013-7444-0
28. Boley B, Weiner J. Theory of thermal stresses. Mineola: Dover Pubns; 1997. p. 272–306.
29. Wang H, Singh RN. Thermal shock behaviour of ceramics and ceramic composites. Int Mater Rev. 1994;39:228–44. https://doi.org/10.1179/imr.1994.39.6.228
30. Wang L, Zhou X, Wei X. Heat conduction: mathematical models and analytical solutions. Berlin: Springer Verlag; 2008.
31. Ding SQ, Zeng YP, Jiang DL. Thermal shock resistance of in situ reaction bonded porous silicon carbide ceramics. Mater Sci Eng A. 2006;425:326–9. https://doi.org/10.1016/j.msea.2006.03.075
32. Kobayashi AS. Dynamic fracture of ceramics and ceramic composites. Mater Sci Eng A. 1991;143:111–7. https://doi.org/10.1016/0921-5093(91)90730-B

SUPPORTING INFORMATION

Additional supporting information can be found online in the Supporting Information section at the end of this article.

How to cite this article: Zuo C, Li Q, Wang Q, Li Y, Li L, Wei J, et al. Effect of material parameters on thermal shock crack of ceramics calculated by phase-field method. J Am Ceram Soc. 2022;105:7649–7657. https://doi.org/10.1111/jace.18720